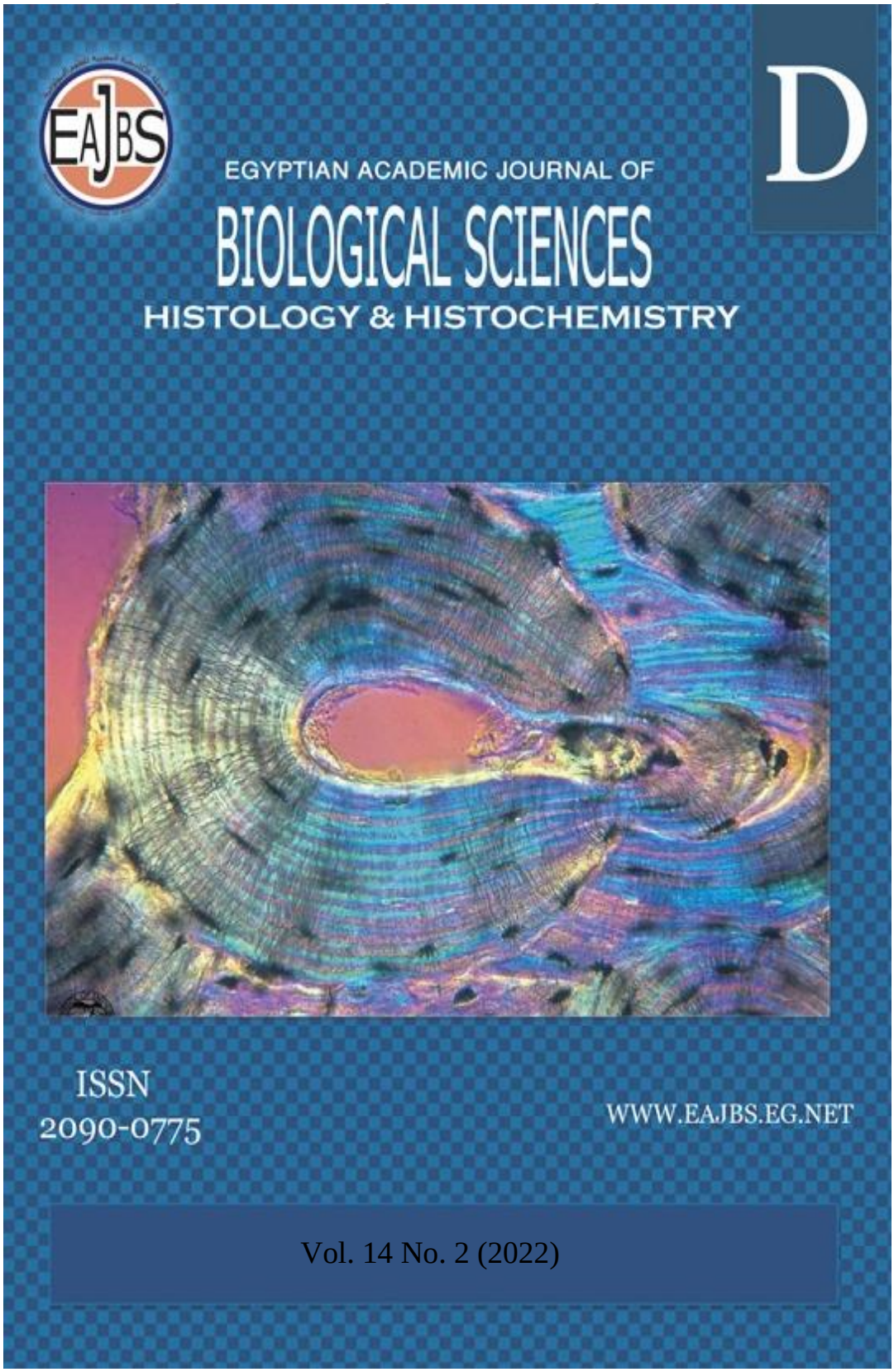

Citation: Egypt. *Acad. J. Biolog. Sci. (D-Histology and histochemistry) Vol.14(2) pp61-84(2022)*
DOI: 10.21608/EAJBSD.2022.264621

Egypt. Acad. J. Biolog. Sci., 14(2): 61-84 (2022)

Egyptian Academic Journal of Biological Sciences
D. Histology & Histochemistry
ISSN 2090 – 0775
http://eajbsd.journals.ekb.eg

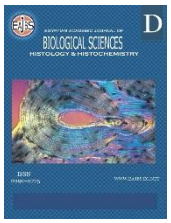

Possible Protective Role of Nanoselenium against Potassium Dichromate-Induced Splenic Toxicity in Adult Male Albino Rat: Histological, Histochemical, Immunohistochemical and Morphometric Study

Reneah R. Bushra and Merry B.K. Shenouda
Department of Human Anatomy and Embryology, Faculty of Medicine, Assiut University, Assiut
E.Mail*:reneah@aun.edu.eg

ARTICLE INFO
Article History
Received:27/8/2022
Accepted:9/10/2022
Available:13/10/2022

***Keywords*:**
Spleen, Potassium Dichromate, Nanoselenium, Albino rat.

ABSTRACT

Introduction: The spleen is a large lymphoid organ that plays an important role in immunity. Potassium dichromium is well-known to be toxic. Nanoselenium is a potent antioxidant trace mineral. The aim of the work was to explore the influence of potassium dichromate on the spleen and the co-administration of nanoselenium against the induced splenic injury. **Material and methods:** 30 adult male albino rats (200-250g) were equally randomly divided into three groups. Group I (the control group) received no treatment. Group II (the chromium-treated group) received potassium dichromate (2 mg/kg b.w. dispersed in 1 ml distilled water) intraperitoneally daily for 2 weeks. Group III (the chromium and selenium-treated group) received nanoselenium (0.5 mg/kg b.w. dissolved in 0.5 ml of phosphate-buffered saline, intraperitoneally) as well as potassium dichromate (2 mg/kg b.w. dispersed in 1 ml distilled water) intraperitoneally daily for 2 weeks. Then, the spleens of all groups were extracted and processed to be studied. **Results:** The chromium-treated group revealed disturbance of the architecture of the white pulp, congestion of the red pulp, deposition of hemosiderin pigments, chromatin condensation of the lymphocytes' nuclei, and markedly dilated rough endoplasmic reticulum of the plasma cells. There were significant increases in the area percentage of collagen fibers deposition and iron staining and a significant decrease in the area percentage of Bcl-2 immune expression. The administration of nanoselenium in Group III ameliorated most of these toxic effects. **Conclusion:** Nanoselenium exhibited a protective role against the toxic effect of potassium dichromate on the spleen.

INTRODUCTION

The spleen is a large lymphoid organ that acts primarily as a massive blood filter. It filters blood-borne antigens and pathogens. It, as a specialized immune organ, plays a major role in adaptive and innate immunity (Aliyu *et al.*, 2021). It also constitutes an essential organ for erythrocyte homeostasis and iron metabolism (Bronte & Pittet, 2013). It is like the lymph node in that it possesses a hilum however, it differs from it in lacking cortex, medulla, and afferent lymphatic vessels. The spleen is divided into red and white pulps, separated from each other by a marginal zone.

The white pulp contains lymphoid elements (Gartner & Hiatt, 2014). Specialized immune cells like macrophages, B-lymphocytes, and natural killer cells populate within them (Aliyu *et al.,* 2021). Injury to the spleen is related directly to immune deficiency (Liu *et al.,* 2022). Heavy metals are hazardous pollutants that negatively affect both human health and the environment (Hosseini *et al.,* 2021). The most frequently found heavy metals in wastewater are nickel, chromium, arsenic, lead, copper, zinc, and cadmium (Jaishankar *et al.,* 2014). Chromium is the 7th most abundant earth's crust element (Xu *et al.,* 2021). Trivalent and hexavalent chromium are considered the most commonly occurring and stable forms of chromium species (Das *et al.,* 2021). Trivalent chromium is essential for metabolic activity and the growth of some microorganisms (Brasili *et al.,* 2020). It is poorly soluble; therefore, it is less toxic than hexavalent chromium (Jiang et al., 2019; Sharma *et al.,* 2020 and Xu *et al.,* 2021).

On the other hand, hexavalent chromium is derived from industrial activities (Genchi *et al.,* 2020). Potassium dichromate ($K_2Cr_2O_7$), which is a soluble form of hexavalent chromium, is widely used in industries like metallurgy, chrome plating, surgical prostheses, stainless steel industries, photography and photoengraving, textile manufacture, wood preservation, and cooling systems (Coetzee *et al.,* 2020). Hexavalent chromium is a soluble and strong oxidizing agent, causing adverse impacts on animals and humans (Nakkeeran *et al.,* 2018). Furthermore, owing to its solubility in the soil and water, it pollutes the ground, water, and food (Des Marais and Costa, 2019; Kumar *et al.,* 2019). It is reduced in the body by substances like glutathione and ascorbate, providing an unstable pentavalent and a stable trivalent chromium (Ray, 2016). During the process of reduction, reactive oxygen species (ROS) are produced (Salama and Elgohary, 2021).

It affects the respiratory tract, hepatic, skin, renal, gastrointestinal, reproductive, and cardiovascular systems (Huang *et al.,* 2019 and Hessel *et al.,* 2021). Chromium-induced oxidative stress induces immune system deterioration and genetic material alteration in humans and animals (El-Demerdash *et al.,* 2021). The Agency for Toxic Substances and Disease Registry ranks chromium as the seventeenth most toxic substance. Besides, it is judged a Group 1 carcinogenic substance by the International Agency for the Research on Cancer, as reported by Loomis *et al.* (2018) and Rahman & Thomas (2021).

Selenium is a critical essential element in immunity, growth, and reproduction (McLaughlin & Gunderson, 2022). Plants are the most important nutritional sources of selenium. They accumulate it naturally and absorb it from the soil, the water, and the atmosphere. Rice, wheat, potatoes, broccoli, apples, and garlic are rich sources of selenium (Jiao *et al.,* 2022). Selenium has antioxidant, anti-inflammatory, and anti-apoptotic effects (Shalihat *et al.,* 2021)**.** Moreover, it protects the body against toxins by increasing antioxidant activity (Kielczykowska *et al.,* 2018). Specifically, selenium can antagonize the heavy metal-induced toxicity in mammals (Lin *et al.,* 2020). Selenium has a protective effect against the splenic toxicity induced by lead (Han *et al.,* 2017), aflatoxin (Chen *et al.,* 2014), cadmium (Chen *et al.,* 2017), and mercuric oxide (Fan *et al.,* 2020).

Furthermore, selenium protects against chromium-induced thyrotoxicity (Mohamed *et al.,* 2016) and nephrotoxicity (Soudani *et al.,* 2010). It alleviates different trace element changes induced by the chromium in the spleen (Chen *et al.,* 2017).

Selenium is particularly important due to its potent prooxidant, antioxidant, anti-inflammatory, and

immunity-boosting capabilities in selenoproteins (Kryukov & Gladyshev, 2002). Nevertheless, a narrow limit exists between adequate selenium intake and toxicity. Selenium antioxidant effects, toxicity, and bioavailability are affected by its concentration, particle size, and chemical form (Hosnedlova *et al.,* 2018). Selenium nanoparticles were recommended because of their remarkably reduced toxicity (Ahmed *et al.,* 2021). Nanoparticles of selenium given to male rats increased the testicular antioxidant action and spermatogenesis more than those from an ordinary form of selenium (Abd-Allah & Hashem, 2015).

The detailed structural studies on the role of selenium in the protection of the spleen against the toxic effects of chromium have not been fully conducted. So, the present work aims at detecting the influence of potassium dichromate on the structure of the spleen and exploring the possible protective role of nanoselenium in the adult male albino rat through histological, histochemical, immunohistochemical, electron microscopic and morphometric studies.

MATERIALS AND METHODS

Chemicals:

Potassium dichromate ($K_2Cr_2O_7$) (CAS No. 7778-50-9) was obtained from Merck (Darmstadt, Germany). Selenium nanoparticles (3–20 nm particles) in metal powder form (CAS No. 7782-49-2) were perceived from the Central Drug House (II0002; PLTD, New Delhi, India).

Experimental Animals:

In this study, a total of 30 adult male albino rats (200–250 g body weight) were used. The rats were taken from the Animal House of the Faculty of Medicine at Assiut University. They were kept at (22.5 °C) with a 12 hours/12 hours light/dark cycle, fed a standard diet, and given unlimited water. They were randomly divided into three equal groups of 10 rats each: Group I (the control group), in which the rats were given no treatment. Group II (chromium-treated group): The rats were given a daily single dose of 2 mg/kg potassium dichromate -dispersed in 1 ml distilled water- intraperitoneally for 2 consecutive weeks (El Bakry & Tawfik, 2014); and Group III (chromium and selenium-treated group): The rats were given a single daily dose of 0.5 mg/kg b.w. nanoselenium -dispersed in 0.5 ml phosphate buffered saline- intraperitoneally (Atteia *et al.,* 2018) as well as potassium dichromate at the same dose and route of administration that was given to Group II for 2 consecutive weeks (El Bakry & Tawfik, 2014). All the experimental procedures were conducted according to the International Guidelines for the Care and Use of Laboratory Animals.

I. Histological Study:

At the end of the experiment, the rats were sacrificed, and each spleen was extracted and cut into two divisions. One part was processed for the light microscopic study, and the other part was processed for the electron microscopic study.

I.1. Light Microscopic Study:

The splenic pieces were fixed with 10% formalin. They were then processed to produce paraffin sections of 5 um thickness. Sections were stained with hematoxylin and eosin (H&E) to study the general architecture of the spleen and Masson's Trichrome to detect the collagen fibers (Bancroft & Layton, 2012). The stained slides were examined and photographed using an Olympus digital camera (Olympus DP27-Japan) installed on an Olympus microscope (Olympus CX41, Tokyo, Japan).

I.2. Electron Microscopic Study:

The specimens of the spleen were cut into about 1 mm^3 cube and fixed in 4% glutaraldehyde and then in 1% osmium tetroxide. Semithin sections of about 0.5-1 um thickness were stained with toluidine blue, examined, and photographed. Ultrathin sections of 50–80 nm thickness were contrasted with uranyl acetate and lead citrate (Woods & Stirling, 2019). Examination and photographing of the sections were done

using the Jeol-JEM-100 CXII transmission electron microscope (Tokyo, Japan) at the Electron Microscopic unit of Assiut University.

II. Histochemical Study:

To detect the intracellular iron accumulation in the spleen, a Prussian blue stain was used as a specific histochemical reaction displaying the iron biodistribution profile. The demonstration of the soluble form of iron was observed in the form of light blue patches, while hemosiderin was observed in the form of dark blue patches. The sections were deparaffinized and rehydrated. For 20 minutes, the sections were stained with 1% freshly prepared potassium ferrocyanide, ($K_4[Fe(CN)_6]$-Sigma Aldrich), and 2% HCl. Then, they were counterstained for 5 minutes with neutral red (Sigma Aldrich) (Orchard, 2019).

III. Immunohistochemical Study:

Immunohistochemical study was done to detect the Bcl-2 (anti-apoptotic protein) expression of the spleen of the different groups. The splenic sections were fixed in formalin, embedded in paraffin, and cut at a thickness of 4 um. Then, they were incubated with an anti-Bcl-2 antibody (rabbit polyclonal antibody, 1/100 dilution, Abcam) overnight. After washing with PBS, incubation of the sections with biotinylated secondary antibody was done for 1 hour at room temperature. Then, the sections were incubated with streptavidin-horseradish peroxidase for ten minutes, then washed with PBS. Diaminobenzidine (DAB)–hydrogen peroxide was applied to localize and visualize the immunoreaction. Then, these sections were counterstained by Mayer's hematoxylin. Finally, they were dehydrated, cleared, and mounted (Sanderson et al., 2019).

IV. Morphometric Study:

The mean ± standard error of the mean (SE) of the area percentage of the collagen fibers of the Masson's Trichrome-stained sections, the area percentage of iron staining by Prussian blue, and the area percentage of Bcl-2 immune expression were obtained in non-overlapping ten fields in Masson's Trichrome and Prussian Blue-stained slides at X200 magnification and Bcl2-immunostained slides at X400 magnification of five rats of each group. Analysis of each photographed field was done using Image J software (National Institute of Health, USA Java 1.8.0-66 (32-bit) (Schneider et al., 2012).

Statistical Analysis:

The obtained measurements were analyzed using SPSS software version 25 (SPSS Inc., Chicago, IL, USA). The data were compared by the analysis of variance (ANOVA) test, followed by the Tukey post hoc test. The differences were considered statistically significant when the p-value was < 0.05.

RESULTS

I. Histological Results:

I.1. Light Microscopic Results:

I.1.a. Hematoxylin and Eosin Results:

The splenic sections of the control rats (Group I) showed the normal architecture of the two components of the parenchyma of the spleen, the white and red pulps (Fig. 1a). The white pulp was composed of lymphatic follicles containing closely packed lymphocytes in addition to the central arterioles that were surrounded by a periarteriolar lymphatic sheath of lymphocytes. The red pulp was demarcated from the white pulp by a marginal zone, which was separated from the lymphatic follicles by a marginal sinus. The red pulp was formed of splenic cords of cells that appeared in the form of networks of cell cords separated by vascular sinuses (Fig. 1b).

The white pulp of the spleen in the chromium-treated group (Group II) showed that most follicles exhibited prominent germinal centers. Thickened trabeculae and numerous acidophilic cells with vesicular nuclei in between the splenic lymphocytes were noticed. Central arterioles surrounded by a periarteriolar sheath appeared somewhat thickened. Red pulps showed dilated, congested blood vessels and multiple

hemosiderin-loaded macrophages (Figs. 1c & 1d).

The splenic sections of the chromium and selenium-treated group (Group III) revealed that the red pulp and the white pulp appeared like those of the control group (Figs. 1e & 1f).

I.1.b. Masson's Trichrome Results:

The splenic sections of the control group showed fine collagen fibers of the capsule, trabeculae, and around the blood vessels (Fig. 2a). The splenic sections of the chromium-treated group (Group II) revealed a marked increase in the collagen fibers of the capsule (Fig. 2b), trabeculae, and around the blood vessels (Fig. 2c) as compared with the control group. Examination of the splenic sections of the chromium and selenium-treated group (group III) revealed that the collagen fibers appeared like those of the control group (Fig. 2d).

I.1.c. Toluidine Blue Results:

Examination of the splenic semithin sections stained with Toluidine Blue of the control group showed that the white pulp exhibited a periarteriolar lymphatic sheath of normal lymphocytes with a rounded nucleus and thin cytoplasm. The periarteriolar sheath was surrounded by a marginal zone and separated from it by a marginal sinus lined by flattened cells. The marginal zone was made up of several rows of cells, the majority of which were macrophages with irregularly outlined large nuclei. Plasma cells with abundant, deeply blue cytoplasm and a round, eccentrically placed nucleus with coarse chromatin arranged in a clock face (cartwheel) pattern were observed. The red pulp consisted of cords of cells and sinusoids, in addition to neutrophils with segmented nuclei (Fig. 3a).

In the chromium-treated group (Group II), the white pulp showed a depletion of cells. Most lymphocytes appeared to have deeply stained irregular nuclei, in addition to many cells with pyknotic nuclei. Moreover, irregularly thickened walls of central arterioles with degenerated areas, a disorganized periarteriolar lymphatic sheath, and an undefined marginal zone were noticed. Empty wide spaces were also observed (Fig. 3b). The red pulp, with most cells appearing with darkly stained irregular nuclei and some appearing with pyknotic nuclei, showed dilated blood sinusoids and extravasation of red blood cells (Fig. 3c).

Semithin sections of the spleen of the chromium and selenium-treated group revealed that most lymphocytes of the white pulp appeared like the control, and the central arteriole had a regular wall. In the red pulp, slightly dilated blood sinusoids and normally appearing plasma cells were observed (Fig. 3d).

I. 2. Electron Microscope Results:

The ultrastructural examination of the splenic sections of the control rats showed lymphocytes that showed nuclei with peripherally condensed chromatin surrounded by a thin rim of cytoplasm. Dendritic cells with euchromatic large nuclei were observed with many cytoplasmic processes that were in contact with lymphocytes. Their cytoplasm contained rough endoplasmic reticulum and abundant ribosomes. The wall of the splenic sinus was lined with elongated spindle-shaped endothelial cells (Fig. 4a). The plasma cells appeared with a large eccentric nucleus containing coarse heterochromatin alternating with euchromatin, giving the characteristic cartwheel appearance. Their cytoplasm revealed parallel arrays of rough endoplasmic reticulum, large Golgi, and mitochondria. Macrophages with a large nucleus and an irregular outline and lysosomal bodies in their cytoplasm were observed (Fig. 4b).

In the chromium-treated group, the lymphocytes showed dilated perinuclear cisterna and mitochondria with destructed cristae. Some cells have a nucleus with an irregular shape and condensed chromatin. The dendritic cells had rarefied cytoplasm, lost cell processes and most organelles, and a dilated rough endoplasmic reticulum.

The macrophages revealed an irregular, dense nucleus. The cytoplasm showed phagosomes and vacuoles (Fig. 5a). The plasma cells had an eccentric, irregular condensed nucleus, and the cytoplasm showed a markedly dilated rough endoplasmic reticulum and vacuolations. There was a disruption of the sinusoidal wall with some degenerated RBCs (Fig. 5b). Aggregations of eosinophils with their characteristic granules were detected (Fig. 5c).

Examination of the splenic ultrathin sections of the chromium and selenium-treated group revealed minimal cell affection. Most lymphocytes appeared with a rounded nucleus surrounded by a thin rim of cytoplasm. The dendritic cells appeared with many cytoplasmic processes that were in contact with lymphocytes. They revealed euchromatic nuclei and abundant ribosomes. Macrophages showed an irregular outline and an eccentric, large nucleus. In addition, lysosomal bodies with heterogenous contents and minute vacuolations were noticed in the cytoplasm (Fig. 6a). Plasma cells appeared nearly like those of the control group with a large eccentric nucleus containing coarse heterochromatin alternating with euchromatin and a well-defined nucleolus. The cytoplasm exhibited residual dilated rough endoplasmic cisternae and some vacuoles in some cells (Fig. 6b). The wall of the splenic sinus was lined with elongated endothelial cells and filled with RBCs (Fig. 6c).

II. Histochemical results:

Prussian Blue-stained splenic sections of the control group showed a mild reaction in the form of bluish spots (Fig. 7a). In the chromium-treated group, a strong reaction with iron deposition was observed in the form of an increased number of light and dark blue colored spots (Fig. 7b). The splenic sections of the chromium and selenium-treated group showed a moderate reaction (Fig. 7c).

III. Immunohistochemical Results:

Immunohistochemically, the white and red pulps of the control group showed a strong Bcl-2 expression in the form of brownish coloration (Fig. 8a). The splenic sections of the chromium-treated group showed a weak Bcl-2 expression (Fig. 8b). The cells of the white pulp and red pulp of the chromium and selenium-treated group revealed a moderate Bcl-2 expression (Fig. 8c).

IV. Morphometric Results:

The mean±SE of the area percentage of the collagen fibers in the Masson's Trichrome-stained sections of the chromium-treated group (6.82 ± 0.51) showed a significant increase when compared to the control group (4.34 ± 0.6). The chromium and selenium-treated group showed no significant difference (4.39 ± 0.63) from the control group (Table and Histogram).

The mean±SE of the area percentage of iron staining by the Prussian Blue in the chromium-treated group (3.88 ± 0.21) showed a significant increase when compared to that of the control group (2.92 ± 0.15). The chromium and selenium-treated group did not differ significantly (2.94 ± 0.19) from the control group (Table and Histogram).

The mean±SE of the area percentage of Bcl-2 immune expression in the chromium-treated group (10.57 ± 0.15) showed a significant decrease when compared to that of the control group (40.56 ± 0.11). The mean±SE of the area percentage of Bcl-2 immune expression in the chromium and selenium-treated group (39.21 ± 0.17) showed no significant difference when compared to that of the control group (Table and Histogram).

Table: The means of the area percentage of collagen fibers by Masson's Trichrome staining, iron staining by Prussian Blue, and Bcl-2 immune expression of the different groups.

	Group I Mean ± SE	**Group II Mean ± SE**	**Group III Mean ± SE**
Area percentage of collagen fibers staining	4.34 ± 0.60	6.82 ±0.51*	4.39 ± 0.63
Area percentage of iron staining	2.92 ± 0.15	3.88 ± 0.21*	2.94 ± 0.19
Area percentage of Bcl-2 immune expression	40.56 ±0.11	10.57± 0.15*	39.21± 0.17

Data are presented as (mean ± SEM)
(*) Significant when compared to the control group ($p < 0.05$)

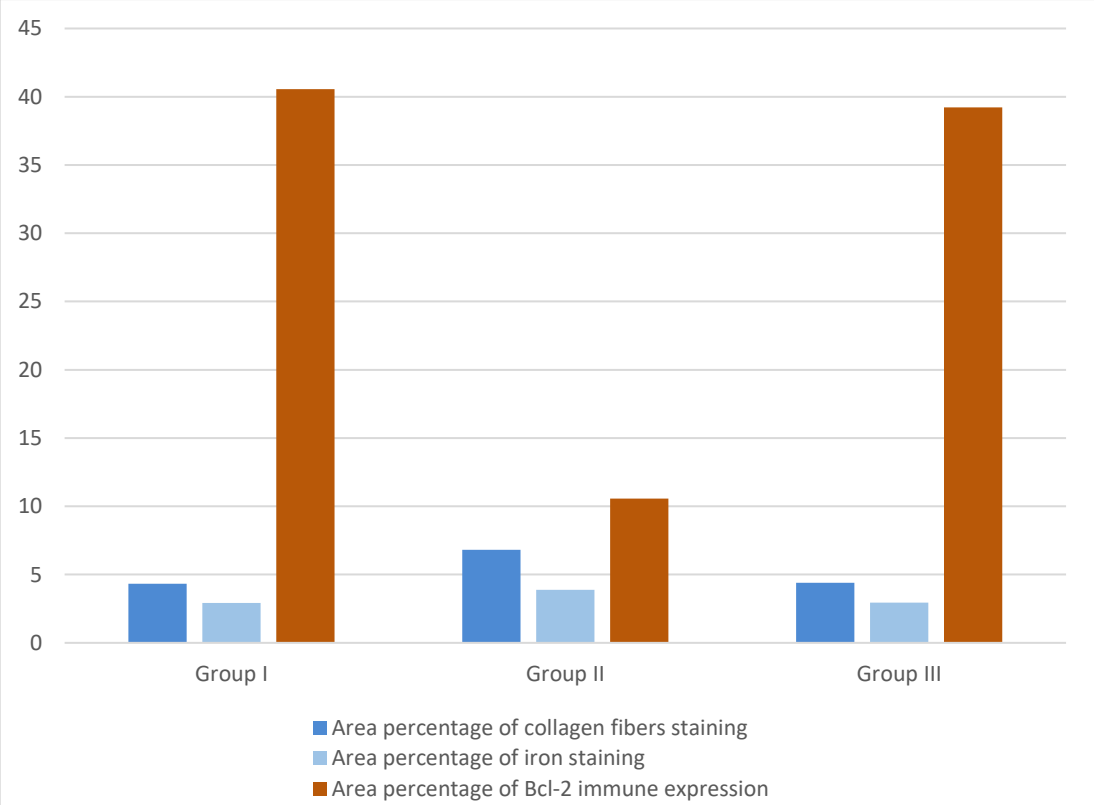

Histogram: Showing the means of the area percentage of collagen fibers staining by Masson's Trichrome, iron staining by Prussian Blue and Bcl-2 immune expression of the different groups.

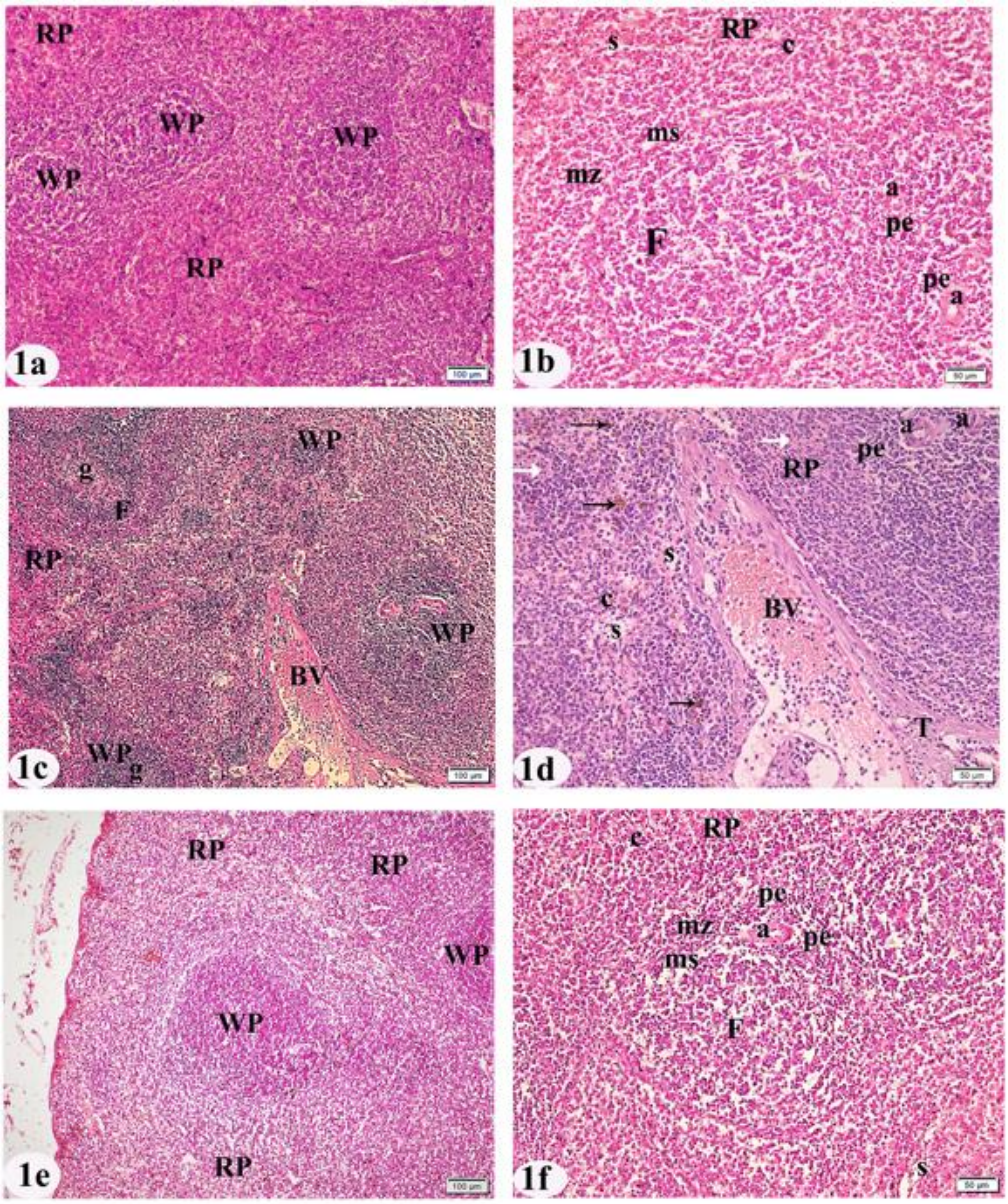

Fig. 1: Photomicrographs of H&E-stained splenic rat sections of the control group (Figs.1a&1b), chromium-treated group (Figs.1c&1d) and selenium and chromium-treated group (Figs.1e&1f) showing; **Fig. 1a:** The white pulp (WP) consists of lymphoid follicles embedded in the highly vascular red pulp (RP) (X100). **Fig. 1b:** The peri-arteriolar lymphatic sheath (pe) is seen around the central arteriole (a). The marginal zone (mz) is differentiated from the red pulp and separated from the lymphatic follicle (F) by the marginal sinus (ms). Normal red pulp (RP) with splenic sinuses (s) and splenic cords (c) is observed (X200). **Fig. 1c:** Lymphatic follicles (F) of the white pulp (WP) appear with prominent germinal centers (g). The red pulp (RP) shows dilated congested blood vessels (BV) (X100). **Fig. 1d:** Apparently thickened trabeculae (T) are noticed. Central arterioles (a) are somewhat thickened and surrounded by a periarteriolar sheath (pe). Numerous acidophilic cells with vesicular nuclei (white arrow) in between the splenic lymphocytes are noticed. The red pulp (RP) shows dilated congested blood vessels (BV) and splenic sinuses (s) between splenic cords (c). Hemosiderin loaden macrophages (black arrow) are noticed (X200). **Fig. 1e:** The white pulp (WP) and the red pulp (RP) retain the normal structure (X100). **Fig. 1f:** The red pulp (RP) shows splenic cords of cells (c) in addition to some dilated sinuses (s). The white pulp consists of lymphatic follicles (F) and central arteriole (a) surrounded by a periarteriolar lymphatic sheath (pe). Note the marginal sinus (ms) and marginal zone (mz) (X200).

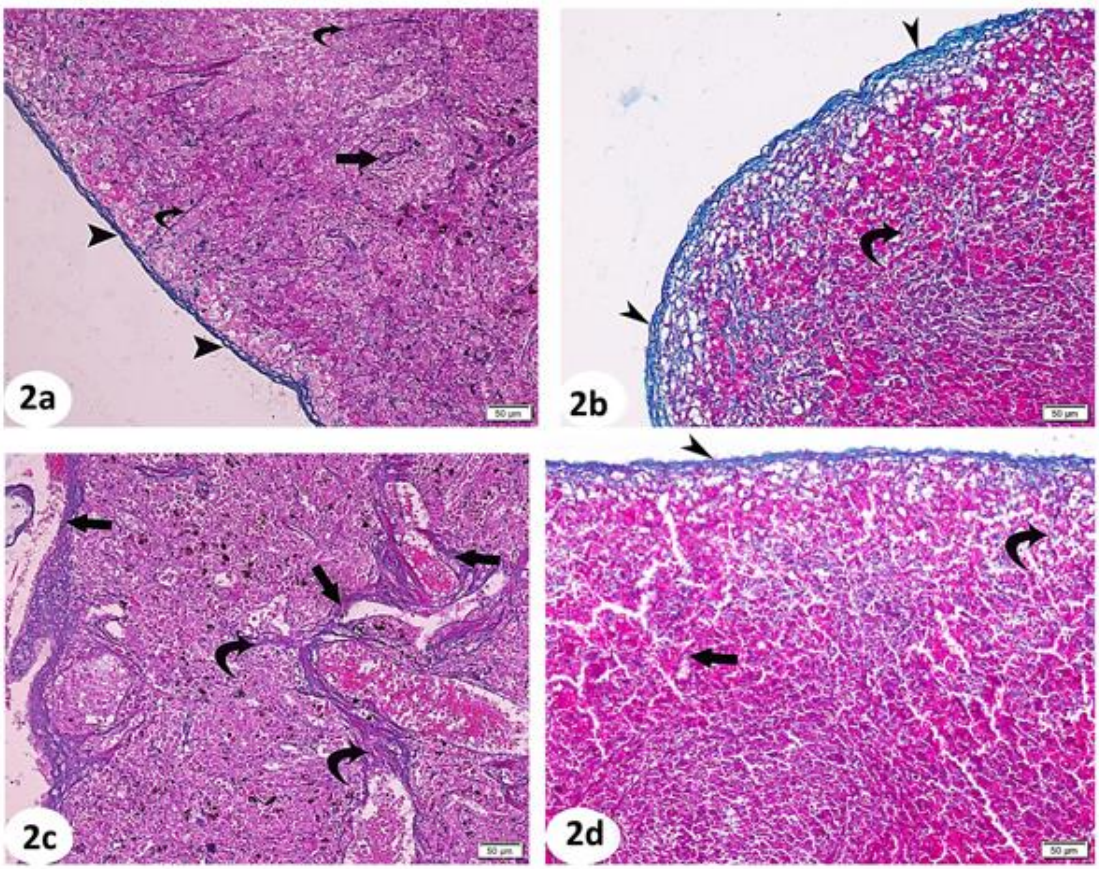

Fig. 2: Photomicrographs of Masson's Trichrome-stained splenic rat sections of the control group (Fig.2a), chromium-treated group (Figs.2b&2c) and selenium and chromium-treated group (Fig.2d) showing; **Fig. 2a:** Fine collagen fibers of the surrounding capsule (arrowhead), around blood vessels (arrow) as well as in the splenic trabeculae (curved arrow) (X200). **Fig. 2b:** Massive collagen fibers deposition in the thickened splenic capsule (arrowhead) and in trabeculae (curved arrow) (X200). **Fig. 2c:** Massive collagen fibers deposition in trabeculae (curved arrow) and around dilated blood vessels (arrow) is observed (X200). **Fig. 2d:** The distribution of collagen fibers appears like that of the capsule (arrowhead), trabeculae (curved arrow) and around blood vessels (arrow) of the control group (X200).

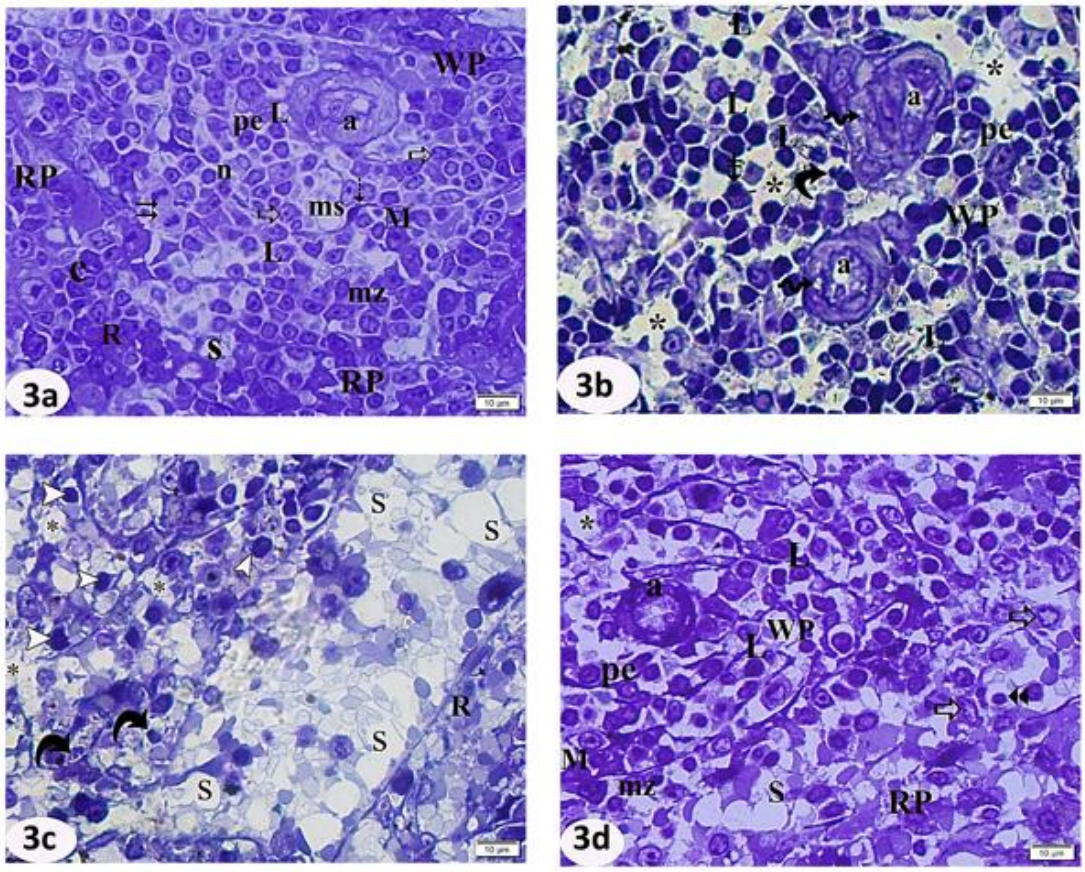

Fig. 3: Photomicrographs of Toluidine Blue-stained semithin sections of the rat spleen of the control group (Fig.3a), chromium-treated group (Figs.3b&3c) and chromium and selenium-treated group (Fig.3d) showing; **Fig. 3a:** The white pulp (WP) exhibits central arteriole (a), periarteriolar lymphatic sheath (pe) consisting of lymphocytes (L) with rounded nuclei. Marginal zone (mz) including macrophages (M) with large nucleus and irregular outline. The periarteriolar lymphatic sheath (pe) is separated from it by a marginal sinus (ms) which is lined by flattened cells (dotted arrow). Plasma cells (arrow) with a rounded, eccentrically placed nucleus displaying coarse chromatin arranged in a clock face pattern and deep blue cytoplasm are observed. The red pulp (RP) is formed of splenic cords (c) and sinusoids (S). Notice the neutrophils (n) with segmented nucleus, mitotic figures (double arrow) and red blood cells (R) (X1000). **Fig. 3b:** The white pulp (WP) appears with most lymphocytes (L) having deeply stained irregular nuclei. Large irregular cells with dense heterogeneous cytoplasm and dense nuclei are noticed (arrow with double stroke). Irregularly thickened walls of central arterioles (a) with degenerated areas (wavy arrow) are noticed. Decreased cellularity of the periarteriolar lymphatic sheath (pe) with empty wide spaces (asterisks) is noticed. Some cells with pyknotic nuclei (curved arrow) are seen (X1000). **Fig. 3c:** The red pulp shows dilated blood sinusoids (S). Most lymphocytes appear with deeply stained irregular nuclei (white arrowhead). Empty wide spaces (asterisks) were present. Extravasated red blood cells are observed (R). Some cells with pyknotic nuclei (curved arrow) are seen (X1000). **Fig. 3d:** Most lymphocytes are with rounded nuclei (L) in the white pulp (WP) including periarteriolar lymphatic sheath (pe). The central arteriole (a) appears with a nearly normal wall. Plasma cells (arrow) with the characteristic nucleus are observed. Note the presence of small empty spaces (asterisk). The red pulp (RP) shows few cells with dense nuclei (double arrowhead) and slightly dilated blood sinusoids (S). Macrophages (M) with large nuclei are observed in the marginal zone (mz) (X1000).

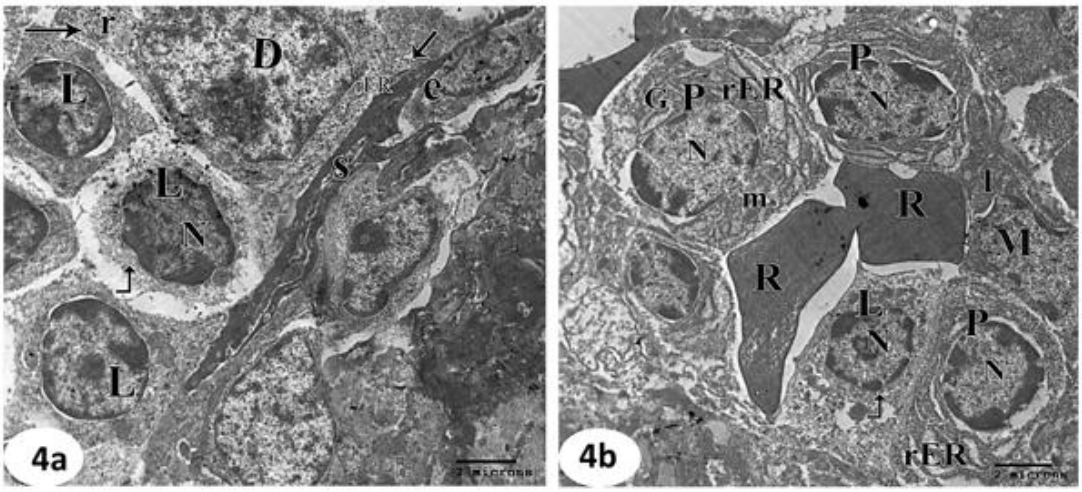

Fig. 4: Electron photomicrographs of the rat spleen of the control group showing; **Fig. 4a:** The lymphocytes (L) have rounded nuclei (N) with peripherally condensed chromatin surrounded by a thin rim of cytoplasm (kinked arrow). A dendritic cell (D) with a euchromatic large nucleus is observed with cytoplasmic processes (arrow). The cytoplasm contains rough endoplasmic reticulum (rER) and abundant ribosomes (r). Note the wall of the splenic sinus (s) that is lined with spindle-shaped elongated endothelial cells (e) (X4800). **Fig. 4b:** The plasma cells (P) appear with a large eccentric rounded nucleus (N) containing coarse heterochromatin alternating with euchromatin giving the characteristic cartwheel appearance. The cytoplasm shows numerous cisternae of rough endoplasmic reticulum (rER), large golgi (G) and mitochondria (m). A macrophage (M) with a large nucleus and irregular outline and lysosomal bodies (l) in the cytoplasm is observed. Note lymphocytes (L) with a thin rim of cytoplasm (kinked arrow) and red blood cells (R) (X4800).

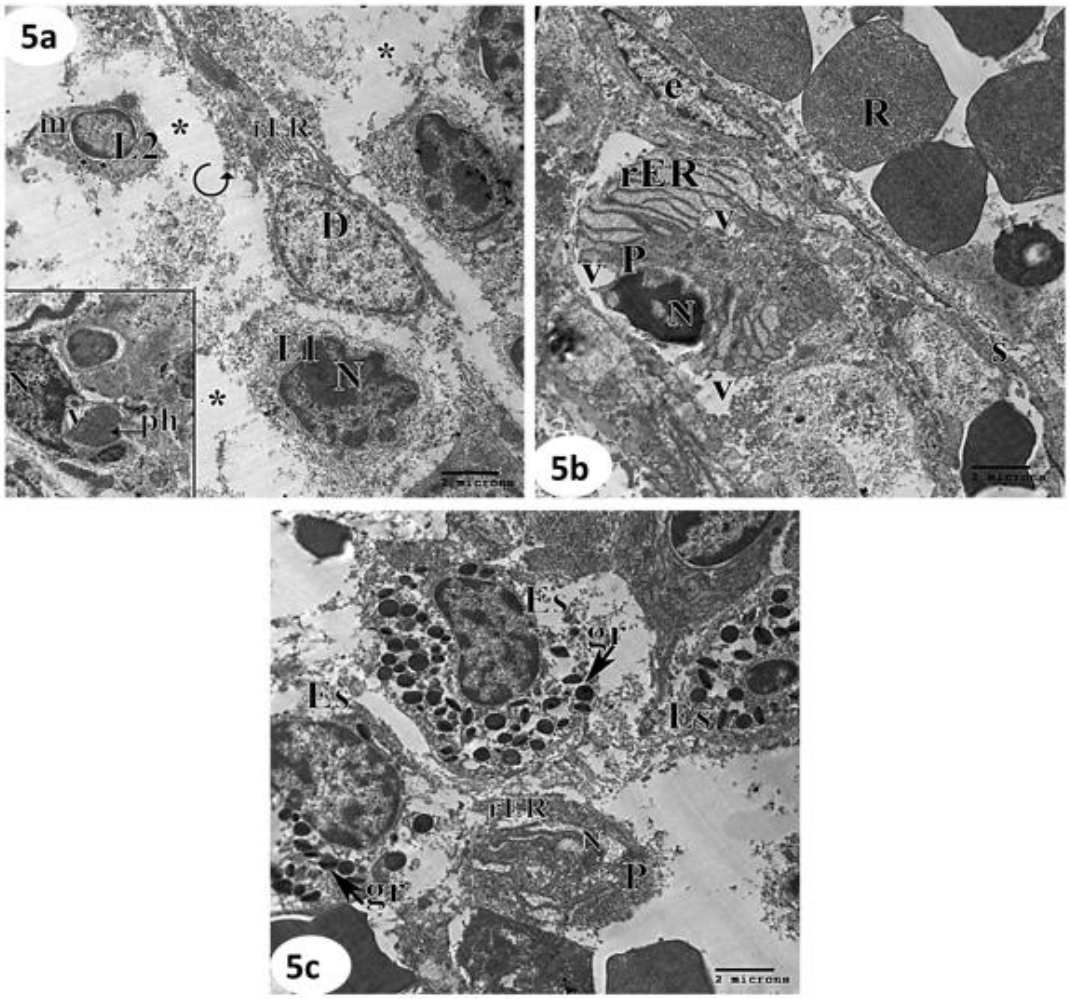

Fig. 5: Electron photomicrographs of the rat spleen of the chromium-treated group showing; **Fig. 5a:** A Lymphocyte (L1) has an irregular nucleus with condensed chromatin (N). Another lymphocyte (L2) has dilated cisternae (double dotted arrow) around the shrunken nucleus and mitochondria (m) with destructed crista. The dendritic cell (D) with rarefied cytoplasm and lost processes (rounded arrow) with loss of most organelles and dilated rough endoplasmic reticulum (rER). Empty spaces are observed (*). **Inset:** Macrophages with irregular dense nucleus (N*). The cytoplasm showed phagosomes (ph) and vacuoles (v) (X4800). **Fig. 5b:** Plasma cell (P) shows eccentric irregular condensed nucleus (N). The cytoplasm shows markedly dilated rough endoplasmic reticulum (rER), and vacuoles (v). There is a disruption in the sinusoidal wall (s). Note the elongated endothelial cell lining (e). Some degenerated RBCs (R) are observed (X4800). **Fig. 5c:** Aggregations of eosinophils (Es) with their characteristic granules (gr) are observed. Note a plasma cell (P) with a condensed nucleus (N) and dilated rough endoplasmic reticulum cisternae (rER) (arrow) (X4800).

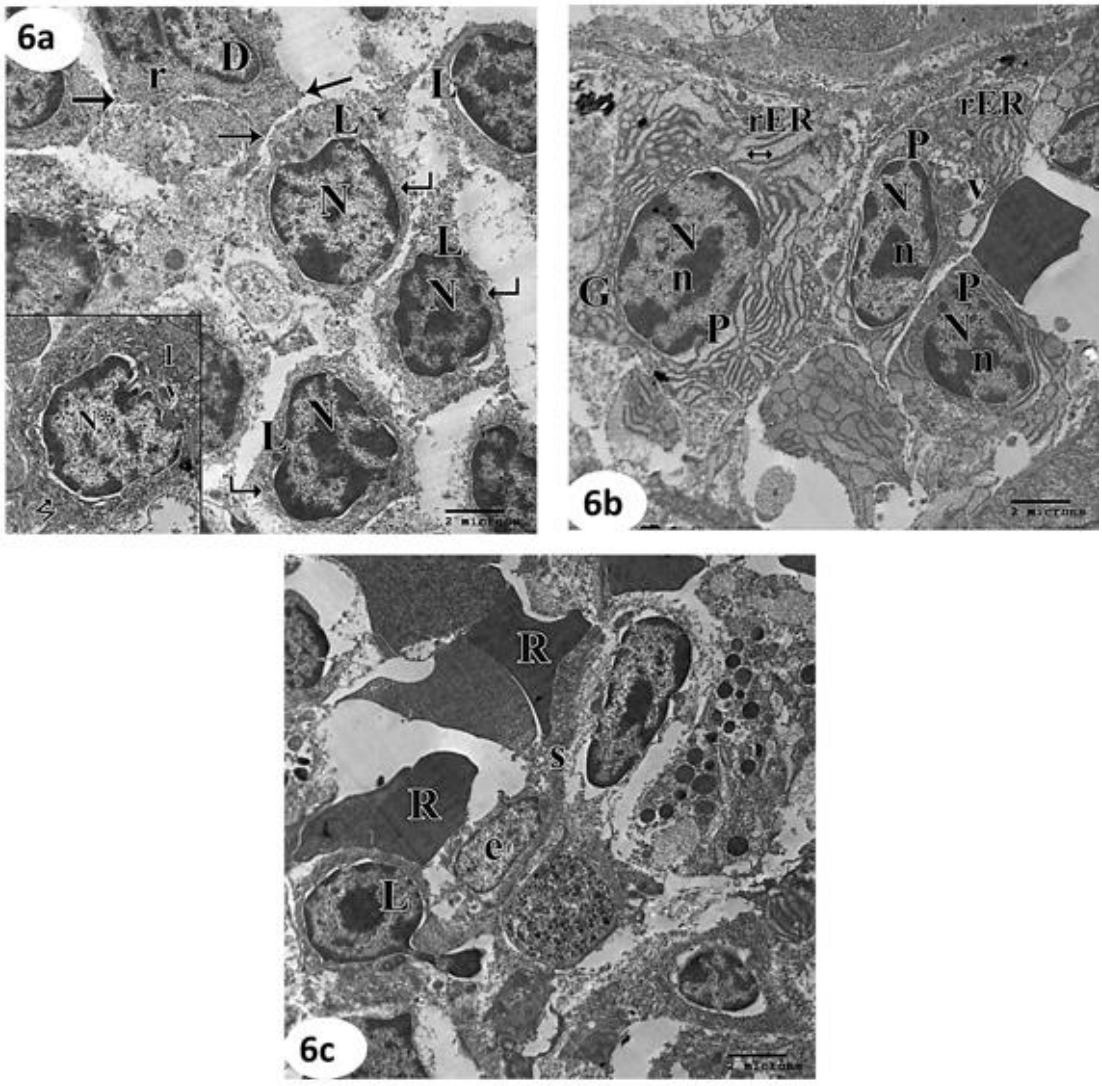

Fig. 6: Electron photomicrographs of the spleen of the chromium and selenium-treated group showing; **Fig. 6a:** Most lymphocytes (L) appear with a rounded nucleus (N) surrounded by a thin rim of cytoplasm (kinked arrow). A dendritic cell (D) with a euchromatic nucleus, cytoplasmic processes (arrows) in contact with lymphocytes and abundant ribosomes (r) are observed. **Inset:** A macrophage with an eccentric large nucleus (N*) and irregular outline (zigzag arrow). Lysosomal bodies (l) with heterogenous contents and minute vacuolations (V) are noticed in the cytoplasm (X4800). **Fig. 6b:** Plasma cells (P) appear with a large eccentric nucleus (N) containing coarse heterochromatin alternating with euchromatin and well-defined nucleolus (n), abundant rough endoplasmic reticulum (rER) and Golgi apparatus (G). Note the presence of some dilated rough endoplasmic reticulum cisternae (double-sided arrow) and some residual vacuoles (v) (X4800). **Fig. 6c:** The sinusoidal wall (S) is lined with an elongated endothelial cell (e). Note a penetrating lymphocyte (L) and red blood cells (R) (X4800).

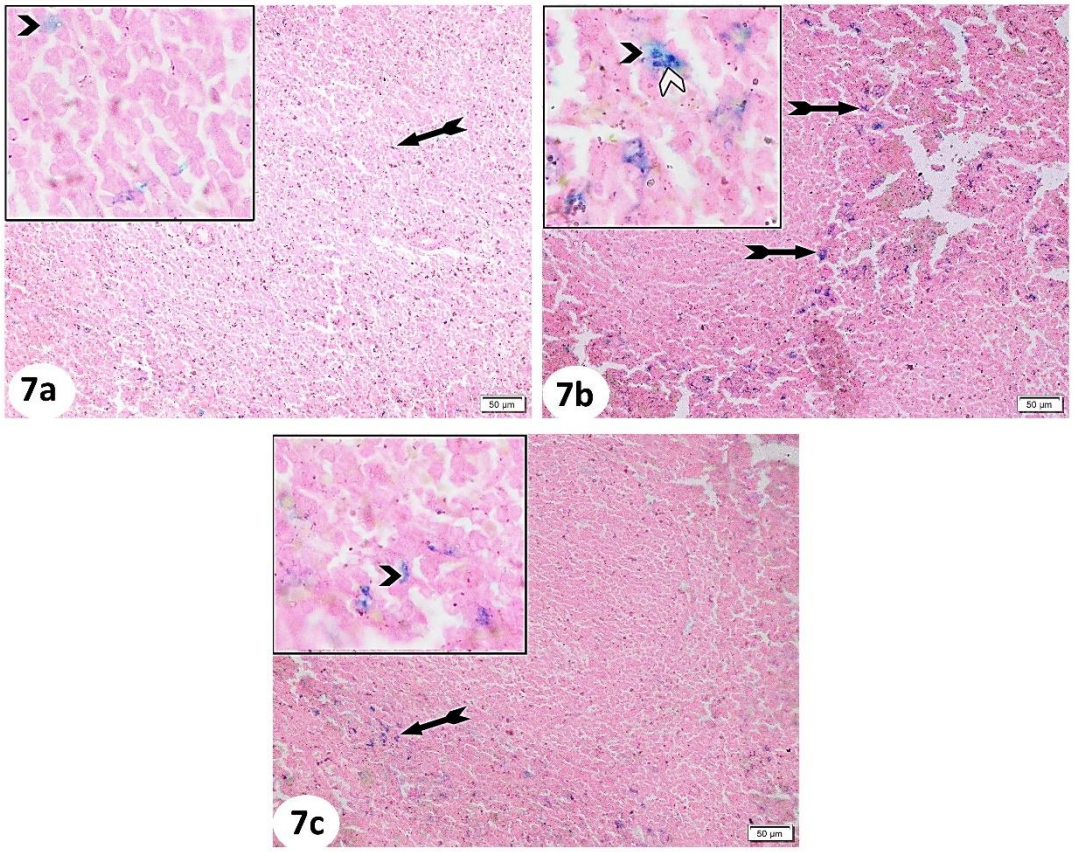

Fig. 7: Photomicrographs of Prussian Blue-stained rat splenic sections of the control group (Fig.7a), chromium-treated group (Fig.7b) and chromium and selenium-treated group (Fig.7c) showing; **Fig. 7a:** Mild reaction in the form of blue staining (tailed arrow) is observed (X200). **Inset:** shows a higher magnification of iron deposition (chevron) (X1000). **Fig. 7b:** Strong reaction with numerous cells with intense blue color (tailed arrow) is noticed. **Inset:** shows a higher magnification of iron deposition with a dark blue (white chevron) and light blue color (black chevron) (X1000). **Fig. 7c:** Moderate reaction (tailed arrow) is seen (X200). **Inset:** shows a higher magnification of iron deposition (chevron) (X1000).

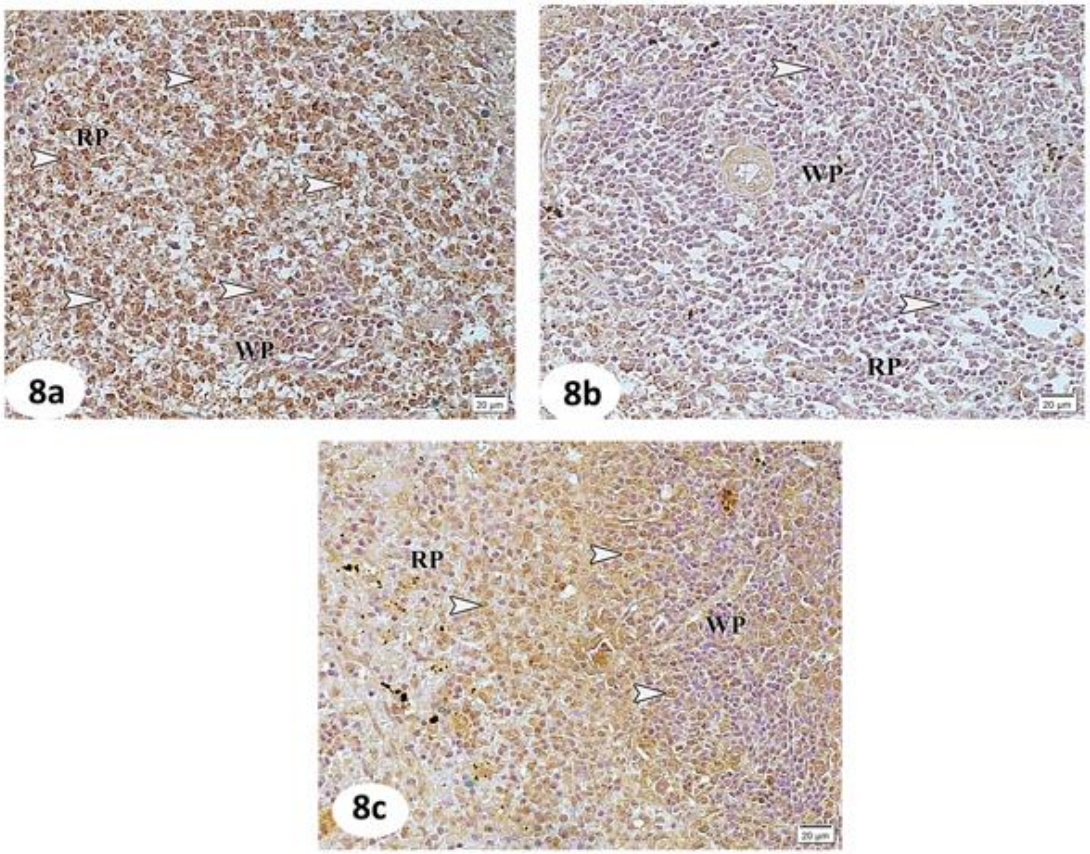

Fig. 8: Photomicrographs of Bcl-2 immuno-stained rat splenic sections of the control group (Fig.8a), chromium-treated group (Fig.8b) and chromium and selenium-treated group (Fig.8c) showing: **Fig. 8a:** A strong positive immunoreaction for Bcl-2 (arrowheads) in the red pulp (RP) and white pulp (WP) is observed. **Fig. 8b:** A weak positive immunoreaction for Bcl-2 (arrowheads) in the red pulp (RP) and white pulp (WP) is observed. **Fig. 8c:** A moderate positive immunoreaction for Bcl-2 (arrowheads) in the red pulp (RP) and white pulp (WP) is observed (X400).

DISCUSSION

The immune system is a well-known critical target for many xenobiotics of organic and inorganic origin (Karaulov *et al.*, 2022). By light microscopic examination of the present study, prominent germinal centers and numerous acidophilic cells with vesicular nuclei in-between the splenic lymphocytes were observed in the white pulp of the chromium-treated group. This finding was reported by Karaulov *et al.* (2022) who associated it with an increased number of B-lymphocytes as a hyperplastic reaction in addition to the accumulation of macrophages because of the chromium exposure.

Multiple hemosiderin-loaded macrophages were found in the chromium-treated group's splenic specimens. This result was in accordance with that of Khalil *et al.* (2013), who observed the red pulp brown pigments of hemosiderosis in the rat spleen exposed to hexavalent chromium. Hemosiderin deposition is typically caused by phagocytosis of extravasated erythrocytes. Iron is released from the haemoglobin of these phagocytosed erythrocytes and stored in ferritin. The ferritin is partially degraded, stored, and converted to hemosiderin in the spleen. As hemosiderin is considered the insoluble form of iron, it was demonstrated by H & E staining however, the soluble form, ferritin, wasn't (Guindi, 2011).

The semithin sections of the chromium-treated group in the present work revealed dilated, congested blood vessels of the red pulp in addition to widening and congestion of the splenic sinuses. This observation was consistent with the observations of Chakraborty *et*

al. (2022) on chromium toxicity in the lung, liver, and kidney. Salama & Elgohary (2021) attributed it to the inflammatory effects of potassium dichromate.

Also, some degeneration of the wall of the central arteriole was observed in the semithin sections of the chromium-treated group of the present work. This observation was in agreement with that of Banu *et al.* (2017), who observed that hexavalent chromium increased the vascular endothelium apoptosis of the endometrium, yolk sac, and trophoblasts by p53 and caspase-3-dependent pathways. A study by Cao *et al.* (2019) proved that chromium induces human umbilical vein endothelial cell apoptosis.

The chromium-treated rat splenic semithin sections of the present work exhibited the appearance of empty spaces in the white pulp, including the periarterial lymphatic sheath, and this could be explained by the suppressed proliferation of B cells and T cells caused by chromium (Chen *et al.*, 2014). Some cells with pyknotic nuclei were observed. These findings were in harmony with a study by Shaw *et al.* (2019), who observed vacuolization of the cytoplasm and extensive pyknotic nuclei formation in the hepatocytes of zebrafish treated with hexavalent chromium.

The present study demonstrated that lymphocytes and dendritic cells of the chromium-treated animals showed marked ultrastructural changes. Lymphocytes showed dilated peri-nuclear cisterna. Some cells have a nucleus with an irregular shape and a condensation of chromatin. Khalil *et al.* (2013) reported similar findings and observed T- and B- lymphocytic necrosis in the $K_2Cr_2O_7$-treated group. These observations could be explained by the reaction of chromium ions with the proteins of the lymphocytic cell surface, causing their injury. So, it alters the cells' responses to various stimuli and deteriorates their cell-mediated and humoral immune functions. Furthermore, when chromium is internalized within the cell, it reacts with the proteins involved in the replication (Qian *et al.*, 2013).

The dendritic cells, as well, appeared with a rarefied cytoplasm and loss of most organelles and their processes. It is postulated that the dendritic cells have an essential role in foreign substances' endocytosis and innate immunity (Merad *et al.*, 2013). The degenerative changes observed in this study could be attributed to the toxic effect of chromium. Similar findings were observed in cells of the lung (García-Niño *et al.*, 2015), thyroid (Mohamed *et al.*, 2016), and liver cells (Tian *et al.*, 2018) upon chromium exposure.

An aggregation of eosinophils was observed in the chromium-treated group in the present work. A similar finding was observed by El-Shenawy *et al.* (2017), who studied the alterations induced in the spleen after treatment with dimethyl-nitrosamine and suggested that these alterations were due to its harmful action as well as the reaction of the affected tissue, expressed by increased activity of plasmocytes, macrophages, eosinophils, neutrophils, and monocytes. Crăciunaş *et al.* (1996) indicated that the releasing of these cells is considered a protective reaction of the spleen against noxious drug exposure.

In the present study, degeneration of the splenic red blood cells was observed by transmission electron microscopic examination of the chromium-treated group. This was in line with Husain & Mahmood (2017), who reported that potassium dichromate enhanced ROS, lowered the antioxidant power, and impaired the antioxidant

enzymes leading to the destruction of the erythrocytic membrane.

This study found that the chromium-treated group had a significantly higher mean area percentage of collagen fibers deposition when compared with that of the control group. These observations can be explained in light of the fact that both parenchymal and capsular splenic fibrosis can occur as a reparative process following injury or inflammation (Elmore, 2006), in addition to the reported fibrogenic effects observed in the chromium-induced liver (Yan *et al.,* 2020) and renal toxicities (Khalaf *et al.,* 2020).

In comparison to the control group, a significant rise in the mean Prussian Blue staining area percentage was seen in the chromium-treated group. This finding could be attributed to the hemosiderin deposition due to abnormal erythrocyte damage induced by chromium, as stated by Kapoor *et al.* (2022).

The current study demonstrated that Bcl-2 expression was significantly lower in the chromium-treated group than that in the control group. This morphometric finding comes in parallel to the immunohistochemical results and could be attributed to the activation of the apoptosis of the mitochondrial pathway and downregulation of Bcl-2 due to chromium toxicity, as mentioned by Abdeen *et al.* (2019), Liu *et al.* (2022), and Zhao *et al.* (2022).

The present study's co-administration of nanoselenium and chromium improved the splenic histopathological alterations, resulting in the restoration of the typical splenic architecture. Amraoui *et al.* (2018) found comparable outcomes while demonstrating the antioxidant efficacy of selenium against Bisphenol A-induced oxidative stress in albino rats. The ability of nanoselenium particles to modify the expression of Bcl-2 and Bcl-2-associated X protein (Bax), hence lowering the ratio of Bax/Bcl-2, the primary index for apoptosis, also offered evidence for their anti-apoptotic characteristics, according to Wang *et al.* (2019). Also, selenium nanoparticles were proven to increase enzymatic antioxidant activity and reduce lipid peroxidation (Gemma *et al.* 2006).

Immunohistochemically, it was demonstrated that the co-administration of nanoselenium with chromium in the present study increased the splenic Bcl-2 expression, and this was confirmed morphometrically. According to similar findings by Yuan *et al.* (2020), nanoselenium can inhibit apoptosis via modulating anti-apoptotic proteins, boosting anti-apoptotic indicators, and reducing pro-apoptotic markers.

In addition, selenium co-administration with chromium in this study induced a statistically significant decrease in the area percentage of collagen fibers deposition as compared with the chromium-treated group. A similar result was observed by Farag & El-Shetry (2020). According to Shalihat *et al.* (2021), this result may be related to selenium's anti-inflammatory properties.

The mean area percentage of iron staining by Prussian Blue of the chromium and selenium-treated group of the present study did not differ significantly from the control group. This observation could be explained by the antioxidant property of selenium based on a previous study by Soudani *et al.* (2011), who reported that co-administration of selenium with $K_2Cr_2O_7$ restored increases protein carbonyl and malondialdehyde levels and decreased vitamin C, non-protein thiol, glutathione, and sulfhydryl levels to near-normal values. And thus, preventing chromium-induced erythrocyte damage.

Conclusion

Hexavalent chromium has a toxic effect on the spleen. So, it is convenient to decrease the exposure to it as much as possible. Selenium nanoparticles, which are potent antioxidants, may have a protective role against chromium-induced splenic toxicity

Conflict of interest

The authors report no conflict of interest.

Ethical Statements:

This study was carried out in strict accordance with the International Guidelines for the Care and Use of laboratory Animals. The experimental protocol was approved by the Ethics Committee at the Faculty of Medicine, Assiut University, Assiut, Egypt (Approval number: IRB17300839).

REFERENCES

Abd-ALLah, S. and Hashem, K. S. (2015). Selenium nanoparticles increase the testicular anti-oxidant activity and spermatogenesis in male rats as compared to ordinary selenium. *International Journal of Advanced Research* , 3: 792-802.

Abdeen, A., Abou-Zaid, O. A., Abdel-Maksoud, H. A., Aboubakr, M., Abdelkader, A., Abdelnaby, A., Abo-Ahmed, A. I., El-Mleeh, A., Mostafa, O., Abdel-Daim, M., and Aleya, L. (2019). Cadmium overload modulates piroxicam-regulated oxidative damage and apoptotic pathways. *Environmental science and pollution research international*, *26*(24): 25167-25177.

Ahmed, Z. S. O., Galal, M. K., Drweesh, E. A., Abou-El-Sherbini, K. S., Elzahany, E. A. M., Elnagar, M. M., and Yasin, N. A. E. (2021). Protective effect of starch-stabilized selenium nanoparticles against melamine-induced hepato-renal toxicity in male albino rats. *International Journal of Biological Macromolecules*, *191*(June): 792-802.

Aliyu, M., Zohora, F. and Saboor-Yaraghi, A. A., (2021). Spleen in innate and adaptive immunity regulation. *AIMS Allergy and Immunology*, 5 (1): 1-17.

Amraoui, W., Adjabi, N., Bououza, F., Boumendjel, M., Taibi, F., Boumendjel, A., Abdennour, C. and Messarah, M. (2018). Modulatory Role of Selenium and Vitamin E, Natural Antioxidants, against Bisphenol A-Induced Oxidative Stress in Wistar Albinos Rats. *Toxicological research*, *34*(3): 231-239.

Ateia, H. H., Arafa, M. H. and Prabahar, K. (2018). Selenium tnanoparticles prevents lead acetate induced hypothyroidism and oxidative damage of thyroid tissues in male rats through modulation of selenoenzymes and suppression of miR-224. *Biomedicine and Pharmacotherapy*, 99: 486–491.

Bancroft, J. D. and Layton C. (2012). The hematoxylin and eosin, Connective and mesenchymal tissues with their stains. In: Suvarna SK, Layton C and Bancroft JD, editors. Bancroft's Theory and Practice of Histological Techniques. 7th edition, Churchill Livingstone, Philadelphia. pp. 173-212.

Banu, S. K., Stanley, J. A., Sivakumar, K. K., Arosh, J. A., Taylor, R. J., and Burghardt, R. C. (2017). Chromium VI − Induced developmental toxicity of placenta is mediated through spatiotemporal dysregulation of cell survival and apoptotic proteins. *Reproductive Toxicology*, *68*: 171-190.

Brasili, E., Bavasso, I., Petruccelli, V., Vilardi, G., Valletta, A., Bosco, C.D., Gentili, A., Pasqua, G. and Palma, L. D. (2020). Remediation of hexavalent chromium contaminated water through zero-valent iron nanoparticles and effects on tomato plant growth performance. *Scientific Reports*, 10: 1920.

Bronte, V. and Pittet, M. J. (2013). The spleen in local and systemic regulation of immunity. *Immunity*, 39 (5): 806-818.

Cao, X., Wang, S., Bi, R., Tian, S., Huo, Y., and Liu, J. (2019). Toxic effects of Cr (VI) on the bovine hemoglobin and human vascular endothelial cells: Molecular interaction and cell damage. *Chemosphere*, *222*: 355-363.

Chakraborty, R., Renu, K., Ahmed, M., El-sherbiny, M., Mahmoud, D., Elsherbini, A., Khalid, A., Vellingiri, B., Iyer, M., Dey, A., and Valsala, A. (2022). Biomedicine & Pharmacotherapy Mechanism of chromium-induced toxicity in lungs, liver and kidney and their ameliorative agents. *Biomedicine & Pharmacotherapy*, *151*: 113119.

Chen, K., Peng, X., Fang, J., Cui, H., Zuo, Z., Deng, J., Chen, Z., Geng, Y., Lai, W., Tang, L., and Yang, Q. (2014). Effects of dietary selenium on histopathological changes and T cells of spleen in broilers exposed to aflatoxin B1. *International Journal of Environmental Research and Public Health*, *11*(2): 1904-1913.

Chen, M., Li, X., Fan, R., Cao, C., Yao, H. and Xu, S. (2017). Selenium antagonizes cadmium-induced apoptosis in chicken spleen but not involving Nrf2-regulated antioxidant response. *Ecotoxicology and Environmental Safety*, *145*: 503-510.

Coetzee, J. J., Bansal, N., and Chirwa, E. M. N. (2020). Chromium in Environment, Its Toxic Effect from Chromite-Mining and Ferrochrome Industries, and Its Possible Bioremediation. *Exposure and Health*, *12*(1): 51-62.

Crăciunaş, C., Crăciun, C., Crăciun, V., Dordea, M. and Toader-Radu, M. (1996). Ultrastructural effects of certain cytostatics on rat spleen. *Curr. Probl. and Techn. In Cellular and Molecular Biology*, 1: 311-317.

Das, P.K., Das, B.P. and Dash, P. (2021). Chromite mining pollution, environmental impact, toxicity and phytoremediation: a review. *Environmental Chemistry Letters*,19: 1369-1381

Des Marais, T. L. and Costa, M. (2019). Mechanisms of chromium-induced toxicity. *Current Opinion in Toxicology*, 14: 1-7.

El Bakry, R., and Tawfik, S. (2014). Histological study of the effect of potassium dichromate on the thyroid follicular cells of adult male albino rat and the possible protective role of ascorbic acid

(vitamin C). *Journal of Microscopy and Ultrastructure*, 2(3): 137.

El-Demerdash, F. M., El-Sayed, R. A. and Abdel-Daim, M. M. (2021). Rosmarinus officinalis essential oil modulates renal toxicity and oxidative stress induced by potassium dichromate in rats. *Journal of Trace Elements in Medicine and Biology*, *67:* 126791.

Elmore, S. A. (2006). Enhanced Histopathology of the Spleen. *Toxicologic Pathology*, *34*(5): 648-655.

El-Shenawy, N. S., Hamza, R. Z. and Khaled, H. E. (2017). Protective effect of α–lipoic acid against spleen toxicity of dimethylnitrosamine in male mice: Antioxidant and ultrastructure approaches. *Biomedicine and Pharmacotherapy*, *96*: 459-465.

Fan, R. F., Liu, J. X., Yan, Y. X., Wang, L. and Wang, Z. Y. (2020). Selenium relieves oxidative stress, inflammation, and apoptosis within spleen of chicken exposed to mercuric chloride. *Poultry Science*, *99* (11): 5430-5439.

Farag, A. I. and EL-Shetry, E. S. (2020). Chromium-Induced Hepatotoxicity and Potential Protective Effect of Selenium in Adult Male Albino Rat: A Histological, Immuno-Histochemical and Molecular Study. *The Medical Journal of Cairo University*, *88*(3): 187-196.

García-Niño, W. R., Zatarain-Barrón, Z. L., Hernández-Pando, R., Vega García, C. C., Tapia, E. and Pedraza-Chaverri, J. (2015). Oxidative Stress Markers and Histological Analysis in Diverse Organs from Rats Treated with a Hepatotoxic Dose of Cr(VI): Effect of Curcumin. *Biological Trace Element Research*, 167(1): 130-145.

Gartner, L. P. and Hiatt, J. L. (2014). Lymphoid Tissue. In: BRS Cell Biology and Histology, 7th edition., Chapter 12. Wolters Kluwer. Philadelphia. pp.199-220.

Gemma, F. M., Ana, N. A., Roberto, P. B. and Eliseo, G. (2006). Selenium and coronary heart disease: a meta-analysis. *The American Journal of Clinical Nutrition*, 84 (4): 762-773.

Genchi, G., Sinicropi, M.S., Lauria, G., Carocci, A. and Catalano, A. (2020). The Effects of cadmium toxicity. *International journal of Environmental Research and Public Health*, 17(11): 3782.

Guindi, M. (2011). Hemochromatosis. In: Romil Saxena editor. Practical Hepatic Pathology: A Diagnostic Approach. Ch 14. W.B. Saunders. pp. 177-189.

Han, Y., Li, C., Su, M., Wang, Z., Jiang, N. and Sun, D. (2017). Antagonistic effects of selenium on lead-induced autophagy by influencing mitochondrial dynamics in the spleen of chickens. *Oncotarget*, *8*(20): 33725-33735.

Hessel, E. V. S., Staal, Y. C. M., Piersma, A. H., den Braver-Sewradj, S. P. and Ezendam, J. (2021). Occupational exposure to hexavalent chromium. Part I. Hazard assessment of non-cancer health effects. *Regulatory Toxicology and Pharmacology*, 126: 105048.

Hosnedlova, B., Kepinska, M., Skalickova, S., Fernandez, C.,

Ruttkay-Nedecky, B., Peng, Q., Baron, M., Melcova, M., Opatrilova, R., Zidkova, J., Bjørklund, G., Sochor, J., and Kizek, R. (2018). Nano-selenium and its nanomedicine applications: a critical review. *International journal of nanomedicine*, *13*: 2107-2128.

Hosseini, S. A., Samani, M. R. and Toghraie, D. (2021). Investigating the hexavalent chromium removal from aqueous solution applying bee carcasses and corpses modified with polyaniline. *Scientific Reports*, 11: 19117.

Huang, D., Liu, C., Zhang, C., Deng, R., Wang, R., Xue, W., Luo, H., Zeng, G., Zhang, Q. and Guo, X. (2019). Cr (VI) removal from aqueous solution using biochar modified with Mg/Al-layered double hydroxide intercalated with ethylenediamine tetra acetic acid. *Bioresource Technology*, 276: 127-132.

Husain, N., and Mahmood, R. (2017). Hexavalent chromium induces reactive oxygen species and impairs the antioxidant power of human erythrocytes and lymphocytes: Decreased metal reducing and free radical quenching ability of the cells. *Toxicology and Industrial Health*, *33*(8): 623-635.

Jaishankar, M., Tseten, T., Anbalagan, N., Mathew, B.B. and Beeregowda, K.N. (2014). Toxicity, mechanism and health effects of some heavy metals. *Interdisciplinary toxicology*.7(2): 60-72.

Jiang, B., Gong, Y., Gao, J., Sun, T., Liu, Y., Oturan, N. and Oturan, M.A., (2019.) The reduction of Cr (VI) to Cr (III) mediated by environmentally relevant carboxylic 368 acids: state-of-the-art and perspectives. *Journal of Hazardous Materials*. 365: 205-226.

Jiao, L., Zhang, L., Zhang, Y., Wang, R., Lu, B., and Liu, X. (2022). Transcriptome analysis provides new insight into the distrion and transport of selenium and its associated metals in selenium-rich rice. *Environmental Pollution*, *301*: 118980.

Kapoor, R. T., Bani Mfarrej, M. F., Alam, P., Rinklebe, J., and Ahmad, P. (2022). Accumulation of chromium in plants and its repercussion in animals and humans. *Environmental Pollution*, *301*: 119044.

Karaulov, A. V., Smolyagin, A. I., Mikhailova, I. V., Stadnikov, A. A., Ermolina, E. V., Filippova, Y. V., Kuzmicheva, N. A., Vlata, Z., Djordjevic, A. B., Tsitsimpikou, C., Hartung, T., Hernandez, A. F. and Tsatsakis, A. (2022). Assessment of the combined effects of chromium and benzene on the rat neuroendocrine and immune systems. *Environmental Research*, *207*: 112096.

Khalaf, A. A., Hassanen, E. I., Ibrahim, M. A., Tohamy, A. F., Aboseada, M. A., Hassan, H. M., and Zaki, A. R. (2020). Rosmarinic acid attenuates chromium-induced hepatic and renal oxidative damage and DNA damage in rats. *Journal of biochemical and molecular toxicology*, *34*(11): e22579.

Khalil, S., Awad, A. and Elewa, Y. (2013). Antidotal impact of extra virgin olive oil against genotoxicity, cytotoxicity and

immunotoxicity induced by hexavalent chromium in rat. *International Journal of Veterinary Science and Medicine, 1*(2): 65-73.

Kielczykowska, M., Kocot, J., Pazdzior, M. and Musik, I. (2018). Selenium - A fascinating antioxidant of protective properties. *Advances in Clinical and Experimental Medicine, 27*(2): 245-255.

Kryukov, G. V. and Gladyshev, V. N. (2002). Mammalian selenoprotein gene signature: identification and functional analysis of selenoprotein genes using bioinformatics methods. *Methods in enzymology*, *347*: 84-100.

Kumar, V., Sharma, A., Kaur, P., Sidhu, G.P.S., Bali, A.S., Bhardwaj, R., Thukral, A.K. and Cerda, A. (2019). Pollution assessment of heavy metals in soils of India and ecological risk assessment: a state-of-the-art. *Chemosphere*, 216: 449-462.

Lin, X., Yang, T., Li, H., Ji, Y., Zhao, Y., and He, J. (2020). Interactions Between Different Selenium Compounds and Essential Trace Elements Involved in the Antioxidant System of Laying Hens. *Biological trace element research*, 193(1): 252-260.

Liu, F., Li, X., Bello, B. K., Zhang, T., Yang, H., Wang, K., & Dong, J. (2022). Difenoconazole causes spleen tissue damage and immune dysfunction of carp through oxidative stress and apoptosis. *Ecotoxicology and Environmental Safety*, 237: 113563.

Loomis, D., Guha, N., Hall, A.L. and Straif, K. (2018). Identifying occupational carcinogens: an update from the IARC monographs. *Occupational & Environmental Medicine*, 75 (8): 593-603.

McLaughlin, Q. R. and Gunderson, M. P. (2022). Effects of selenium treatment on endogenous antioxidant capacity in signal crayfish (Pacifastacus leniusculus). *Comparative Biochemistry and Physiology Part C: Toxicology & Pharmacology*, 256: 109324.

Merad, M., Sathe, P., Helft J., Miller, J. and Mortha, A. (2013). The dendritic cell lineage: on-togeny and function of dendritic cells and their subsets in the steady state and the inflamed setting, *Annual Review of Immunology*, 31: 563-604.

Mohamed, H. Z. E., Ragab, I. K. and Ghafeer, H. H. (2016). A histological study on the possible protective effect of selenium against chromium-induced thyrotoxicity in adult male albino rats. *Egyptian Journal of Histology*, 39 (1): 1-11.

Nakkeeran, E., Patra, C., Shahnaz, T., Rangabhashiyam, S. and Selvaraju, N. (2018). Continuous biosorption assessment for the removal of hexavalent chromium from aqueous solutions using Strychnos nux vomica fruit shell. *Bioresource Technology Reports*, 3: 256-260.

Orchard,G. E. (2019). Pigments and minerals. In: Suvarna SK, Layton C and Bancroft JD, editors. Bancroft's Theory and Practice of Histological Techniques. 8th edition, Chapter 14, Churchill Livingstone, Philadelphia. pp. 198-230.

Qian, Q., Li, P., Wang, T., Zhang, J., Yu, S., Chen, T., Yan, L., Song, Y., Liu, X., Gu, Y., Wang, Y. and Jia, G. (2013). Alteration of Th1/Th2/Th17 cytokine profile and humoral immune responses associated with chromate exposure. *Occupational and Environmental Medicine*, 70: 697-702.

Rahman, Z. and Thomas, L. (2021). Chemical-assisted microbially mediated chromium (Cr) (VI) reduction under the influence of various electron donors, redox mediators, and other additives: an outlook on enhanced Cr (VI) removal. *Frontiers in Microbiology*, 11: 619766.

Ray, R. R. (2016). Adverse hematological effects of hexavalent chromium: an overview. *Interdisciplinary Toxicology*, 9(2): 55-65.

Salama, A., and Elgohary, R. (2021). L-carnitine and Co Q10 ameliorate potassium dichromate -induced acute brain injury in rats targeting AMPK/AKT/NF -κβ. *International Immunopharmacology, 101(Pt B): 107867.*

Sanderson, T., Wild, G., Cull, A. M., Marston, J., and Zardin, G. (2019). Immunohistochemical and immunofluorescent techniques. In: Suvarna SK, Layton C and Bancroft JD, editors. Bancroft's Theory and Practice of Histological Techniques. 8th edition, Chapter 19, Churchill Livingstone, Philadelphia. Pp: 337-394.

Schneider, C. A., Rasband, W. S., and Eliceiri, K. W. (2012). NIH Image to ImageJ: 25 years of image analysis. *Nature methods*, 9(7): 671-675.

Shalihat, A., Hasanah, A. N., Mutakin, Lesmana, R., Budiman, A. and Gozali, D. (2021). The role of selenium in cell survival and its correlation with protective effects against cardiovascular disease: A literature review. *Biomedicine and Pharmacotherapy*, *134*: 111125.

Sharma, A., Kapoor, D., Wang, J., Shahzad, B., Kumar, V., Bali, A. S., Jasrotia, S., Zheng, B., Yuan, H. and Yan, D. (2020). Chromium bioaccumulation and its impacts on plants: an overview. *Plants*, 9 (1): 100.

Shaw, P., Mondal, P., Bandyopadhyay, A., and Chattopadhyay, A. (2019). Environmentally relevant concentration of chromium activates Nrf2 and alters transcription of related XME genes in liver of zebrafish. *Chemosphere*, *214*: 35-46.

Soudani, N., ben Amara, I., Sefi, M., Boudawara, T., and Zeghal, N. (2011). Effects of selenium on chromium (VI)-induced hepatotoxicity in adult rats. *Experimental and Toxicologic Pathology*, 63(6): 541-548.

Soudani, N., Sefi, M., Ben Amara, I., Boudawara, T., and Zeghal, N. (2010). Protective effects of Selenium (Se) on Chromium (VI) induced nephrotoxicity in adult rats. *Ecotoxicology and Environmental Safety*, *73*(4): 671-678.

Tian, X., Zhang, H., Zhao, Y., Mehmood, K., Wu, X., Chang, Z., Luo, M., Liu, X., Ijaz, M., Javed, M. T., and Zhou, D. (2018). Transcriptome analysis reveals the molecular mechanism of hepatic

metabolism disorder caused by chromium poisoning in chickens. *Environmental science and pollution research international*, *25*(16): 15411-15421.

Wang, L., Xiao, J.-X., Hua, Y., Xiang, X.-W., Zhou, Y.-F., Ye, L. and Shao, Q.-J. (2019). Effects of dietary selenium polysaccharide on growth performance, oxidative stress and tissue selenium accumulation of juvenile black sea bream, Acanthopagrus schlegelii. *Aquaculture* 503: 389-395.

Woods, A. E. and Stirling, J. W. (2019). Transmission electron microscopy. In: Suvarna SK, Layton C, Bancroft JD, editors. Theory and Practical Histological Techniques. 8th edition, Chapter 21, Churchill Livingstone, Philadelphia. pp. 434-475.

Xu, Z., Xu, X., Yu, Y., Yao, C., Tsang, D.C. W. and Cao, X. (2021). Evolution of redox activity of biochar during interaction with soil minerals: effect on the electron donating and mediating capacities for Cr(VI) reduction. *Journal of Hazardous Materials*. 414: 125483.

Yan, J., Huang, H., Liu, Z., Shen, J., Ni, J., Han, J., Wang, R., Lin, D., Hu, B. and Jin, L. (2020). Hedgehog signaling pathway regulates hexavalent chromium-induced liver fibrosis by activation of hepatic stellate cells. *Toxicology Letters*, *320*: 1-8.

Yuan, X., Fu, Z., Ji, P., Guo, L., Al-Ghamdy, A. O., Alkandiri, A., Habotta, O. A., Moneim, A. E. A., & Kassab, R. B. (2020). Selenium nanoparticles pre-treatment reverse behavioral, oxidative damage, neuronal loss and neurochemical alterations in pentylenetetrazole-induced epileptic seizures in mice. *International Journal of Nanomedicine*, 15: 6339–6353.

Zhao, Y., Zhang, H., Hao, D., Wang, J., Zhu, R., Liu, W., and Liu, C. (2022). Selenium regulates the mitogen-activated protein kinase pathway to protect broilers from hexavalent chromium-induced kidney dysfunction and apoptosis. *Ecotoxicology and Environmental Safety*, *239*: 113629.